PAPER

Highly efficient polymer solar cells cast from non-halogenated xylene/anisaldehyde solution

Christian Sprau,[a] Felix Buss,[b] Michael Wagner,[a] Dominik Landerer,[a] Manuel Koppitz,[a] Alexander Schulz,[a] Daniel Bahro,[a] Wilhelm Schabel,[b] Philip Scharfer[b] and Alexander Colsmann*[a]

Several high performance polymer:fullerene bulk-heterojunction photo-active layers, deposited from the non-halogenated solvents *o*-xylene or anisole in combination with the eco-compatible additive *p*-anisaldehyde, are investigated. The respective solar cells yield excellent power conversion efficiencies up to 9.5%, outperforming reference devices deposited from the commonly used halogenated chlorobenzene/1,8-diiodooctane solvent/additive combination. The impact of the processing solvent on the bulk-heterojunction properties is exemplified on solar cells comprising benzodithiophene-thienothiophene co-polymers and functionalized fullerenes (PTB7:PC$_{71}$BM). The additive *p*-anisaldehyde improves film formation, enhances polymer order, reduces fullerene agglomeration and shows high volatility, thereby positively affecting layer deposition, improving charge carrier extraction and reducing drying time, the latter being crucial for future large area roll-to-roll device fabrication.

Broader context

Organic bulk-heterojunction solar cells are on the cusp of commercialization. Printing and coating techniques are widely considered enablers of low-cost solar module fabrication with excellent carbon footprints. For the transfer of lab-scale processes to an environmentally friendly and sustainable industrial large-scale fabrication of polymer solar cells by printing, non-halogenated solvents and processing additives are mandatory prerequisites. As the choice of solvents is pivotal to the complex formation of the bulk-heterojunction and hence to the device performance, both academia and the solar industry have fostered strong research on "green" device processing in order to advance the market-readiness of organic solar modules.

1. Introduction

Recent efforts to push organic photovoltaics towards market-readiness mainly focused on the development of new photo-active polymers and intensive optimization of lab-scale devices, nowadays yielding power conversion efficiencies (PCEs) beyond 10%.[1] Yet, the main challenge will be the transfer of the optimized lab-scale processes to large-area industrial solar cell fabrication.[2,3] In contrast to lab-processing, the use of non-halogenated, eco-friendly and non-hazardous solvents for the processing of the photo-active layers is pivotal for any industrial fabrication. Common lab-scale research utilizes halogenated solvents, such as chlorobenzene (CB), *o*-dichlorobenzene (*o*-DCB) or chloroform, which typically show excellent solubility of most photo-active polymers. Unfortunately, the large-scale use of those

solvents has a dramatic impact on the environment and is hazardous to the human health. Therefore, a strong need for alternative solvents has been recognized by the community, recently focusing on novel high-performance polymer:fullerene bulk-heterojunction (BHJ) solar cells, deposited from non-chlorinated mono-, bis- or tris-substituted benzene analogues.[4–11] While most reports in the literature have focused on the eco-friendliness of the main solvents, little attention has been paid to solvent additives which are often used to control the film drying in order to yield a favorable nano-morphology. Indisputably, the morphology of organic solar cells depends on the processing conditions and critically determines the basic physical processes in the photo-active layer, including light absorption, exciton dissociation, charge carrier transport, charge carrier extraction and recombination. Typically, solvent additives have a higher boiling point than the main solvent and can show selective solubility of one of the two blend components,[12] with the complex BHJ formation processes still being discussed.[13–16] Most additive studies evolved around the use of alkanedithiols and halogenated alkanes.[12,17] For the deposition of most novel polymer:fullerene

[a] *Light Technology Institute, Karlsruhe Institute of Technology (KIT), Engesserstrasse 13, 76131 Karlsruhe, Germany. E-mail: christian.sprau@kit.edu, alexander.colsmann@kit.edu*

[b] *Institute of Thermal Process Engineering, Thin Film Technology, Karlsruhe Institute of Technology (KIT), Kaiserstrasse 12, 76131 Karlsruhe, Germany*

2744 | *Energy Environ. Sci.,* 2015, **8**, 2744–2752

This journal is © The Royal Society of Chemistry 2015

Table 1 Common solvent additives used in previous studies and *p*-anisaldehyde (AA) with the respective hazard classification according to Regulation (EC) No. 1272/2008. Hazard statements are according to the respective material safety data sheet (MSDS) in the current version available from Sigma–Aldrich

Additive	Hazard statements
DIO	H413 chronic aquatic toxicity
CN	H302 acute toxicity, oral H315 skin irritation H319 eye irritation H335 specific target organ toxicity – single exposure H400 acute aquatic toxicity
MN	H302 acute toxicity, oral H315 skin irritation H319 eye irritation H334 respiratory sensitisation H335 specific target organ toxicity – single exposure H411 chronic aquatic toxicity
THN	H315 skin irritation H319 eye irritation H351 carcinogenicity H304 aspiration hazard H411 chronic aquatic toxicity
DPE	H319 eye irritation H411 chronic aquatic toxicity
NMP	H315 skin irritation H319 eye irritation H360 reproductive toxicity H335 specific target organ toxicity – single exposure
AA	None

BHJs, the iodated solvent additive 1,8-diiodooctane (DIO) is used. Alternative additives such as the chlorinated 1-chloronaphthalene (CN) or the non-halogenated 1-methylnaphthalene (MN), 1,2,3,4-tetrahydronaphthalene (THN), diphenyl ether (DPE) and 1-methyl-2-pyrrolidone (NMP) have been studied,[5,7,8,10,18–20] however, all-together disregarding health and environmental hazards (Table 1).

Besides environmental concerns, more volatile solvent additives than DIO may be beneficial for future roll-to-roll processing due to reduced drying times and temperatures.

In this work, we investigate the deposition of various high-performing polymer:fullerene BHJs from the non-halogenated and production relevant solvents *o*-xylene or anisole in combination with the eco-compatible additive *p*-anisaldehyde (AA). The respective solar cells yield PCEs outperforming devices fabricated from common halogenated solvent/additive combinations such as CB and DIO.

2. Experimental

Device fabrication

Organic solar cells were fabricated according to the device architecture depicted in Fig. 1a. Patterned indium tin oxide (ITO, $R_\square \approx 15\ \Omega_\square$) coated glass substrates were cleaned by sequential ultrasonication in acetone and isopropanol (10 min). Then the substrates were transferred into a nitrogen glovebox for the fabrication and characterization process. A zinc oxide (ZnO) electron extraction layer was spin cast from nanoparticle dispersion (Nanograde Ltd, 1 wt% in isopropanol, 4000 rpm, 30 s) and thermally annealed on a hotplate (80 °C, 10 min). Poly[[4,8-bis[(2-ethylhexyl)oxy]benzo[1,2-*b*:4,5-*b*′]dithiophene-2,6-diyl][3-fluoro-2-[(2-ethylhexyl)carbonyl]thieno[3,4-*b*]thiophenediyl]] (PTB7, 1-Material Inc., M_w = 125 kg mol^{-1}, $Đ_M$ = 2.5) and [6,6]-phenyl C$_{71}$-butyric acid methyl ester (PC$_{71}$BM, Solenne, 99%) were dissolved (1:1.5 w/w, polymer concentration 10 g L^{-1}) in either chlorobenzene (CB, anhydrous, 99.8%,), *o*-xylene (anhydrous, 97%) or anisole (anhydrous, 99.7%) and stirred overnight at elevated temperatures (CB: 50 °C, *o*-xylene and anisole: 85 °C). All solvents and additives were used as purchased (Sigma-Aldrich). The solvent additives, either 1,8-diiodooctane (DIO, 98%) or *p*-anisaldehyde (AA, 98%), were then added to the stock solution. The non-filtered warm solution was spun onto the samples (1500 rpm, 60 s) to form the photo-active layer. After initial film drying at room temperature (10 min), the films were annealed on a hotplate (60 °C, 20 min) to remove the residual additive. Then the devices were transferred into a vacuum chamber (base pressure 10^{-6} mbar) to deposit the molybdenum oxide hole extraction layer (MoO$_3$, 10 nm) and the silver top electrode (Ag, 100 nm) by thermal evaporation, using a shadow mask defining
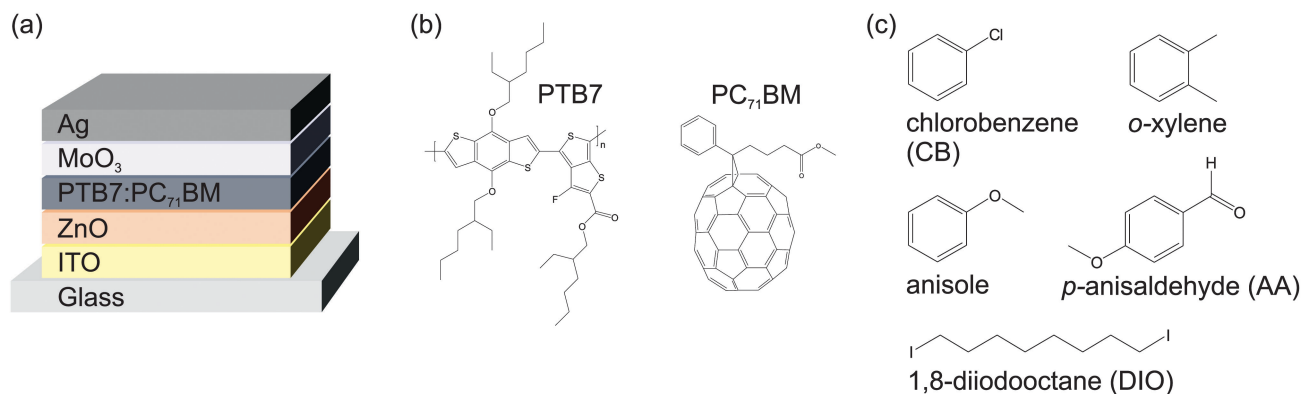
Fig. 1 (a) Solar cell device architecture. (b) Active layer components PTB7 and PC$_{71}$BM. (c) Chemical structures of the solvents and additives investigated in this work.

This journal is © The Royal Society of Chemistry 2015

Energy Environ. Sci., 2015, **8**, 2744–2752 | **2745**

the active solar cell area (3×3.5 mm^2). The same device architecture and fabrication procedure were employed to investigate all other polymer:PC$_{71}$BM photo-active layers. Poly[[4,8-bis[5-(2-ethylhexyl)thiophen-2-yl]benzo[1,2-b:4,5-b′]dithiophene-2,6-diyl]-[3-fluoro-2-[(2-ethylhexyl)carbonyl]thieno[3,4-b]thiophenediyl]] (PTB7-Th, 1-Material Inc., M_w = 108 kg mol^{-1}, $Đ_M$ = 2.5), poly-[[2,7-(5,5-bis-(3,7-dimethyloctyl)-5H-dithieno[3,2-b:2′,3′-d]pyran)-alt-4,7-(5,6-difluoro-2,1,3-benzothiadiazole)]] (PDTP-DFBT, 1-Material Inc., M_w = 37 kg mol^{-1}, $Đ_M$ = 2.4) and poly[[5,6-difluoro-2,1,3-benzothiadiazol-4,7-diyl]-alt-(3,3′′′-di(2-octyldodecyl)-2,2′;5′,2″;5″,2′′′-quaterthiophen-5,5′′′-diyl)]] (PffBT4T-2OD, 1-Material Inc., M_w = 100 kg mol^{-1}, $Đ_M$ = 2.5) were dissolved and mixed with PC$_{71}$BM according to the blend ratios and polymer concentrations listed in Table 4. All solids were sufficiently dissolved in all solvents and the solutions were deposited without filtering. PTB7-Th:PC$_{71}$BM solutions and films were prepared following the PTB7:PC$_{71}$BM deposition protocol. PDTP-DFBT:PC$_{71}$BM solutions were stored overnight on a hotplate (85 °C) and spun (1200 rpm, 60 s; 800 rpm from o-DCB solution) from warm solution (60 °C). PffBT4T-2OD:PC$_{71}$BM solutions were stirred overnight (110 °C) and spun (800 rpm, 120 s) onto warm substrates (solution and substrates were stored on a 95 °C hotplate prior to spin casting) followed by subsequent annealing (80 °C, 5 min).

Characterization

Current density–voltage (J–V) curves were measured using a source-meter unit (Keithley 238) under illumination from a spectrally monitored solar simulator (Oriel 300 W, 1000 W m^{-2}, ASTM AM 1.5G), calibrated by a KG5 filtered silicon reference cell (91150-KG5, Newport). Layer thicknesses were measured using a tactile stylus profiler (Dektak XT, Bruker). Absorbance spectra were recorded using a UV-Vis-NIR spectrophotometer (Cary 5000, Agilent Technologies) in two-beam transmission mode. The respective photo-active layers on glass substrates were prepared following the procedure described above. Atomic force microscopy (AFM, Dimension ICON, Bruker) images were recorded on solar cells next to the top electrodes in tapping mode (TESP tip).

QCM measurements

Quartz Crystal Microbalance (QCM) measurements were carried out at 25 °C in a temperature-controlled chamber equipped with a Q-Sense ALD holder connected to a Q-Sense E1 system. Quartz crystals with a gold surface (QSense QSX301) were cleaned by sequential ultrasonication in toluene (9 min) and ethanol (9 min). Prior to coating, the resonant frequencies of the uncoated crystals were determined. For each drying experiment, the PTB7:PC$_{71}$BM solution (50 μl) was spin coated onto a quartz crystal (3000 rpm, 60 s) under ambient conditions at room temperature. Immediately after coating or after a subsequent heating step on a hot plate (1 min, 60 °C), the crystals were transferred to the measurement chamber, where the drying process of the film was monitored by recording the frequency change $\Delta f_n/n$ of the first five harmonics (n = 1, 3, 5, 7, 9) over time. For the calculation of the areal mass, the

Sauerbrey equation was used:

$$\Delta m = -C\frac{\Delta f_n}{n} \tag{1}$$

where Δm is the difference in areal mass, C is the Sauerbrey constant (17.8 ng cm^{-1} Hz^{-1}) and Δf_n is the measured frequency difference of the n-th harmonic. The equation is valid if the ratio of the change in dissipation and frequency is small (that is $\Delta D_n/(\Delta f_n/n) \ll 4 \times 10^{-7}$ Hz^{-1}),[21] which is fulfilled for all experiments.

3. Results and discussion
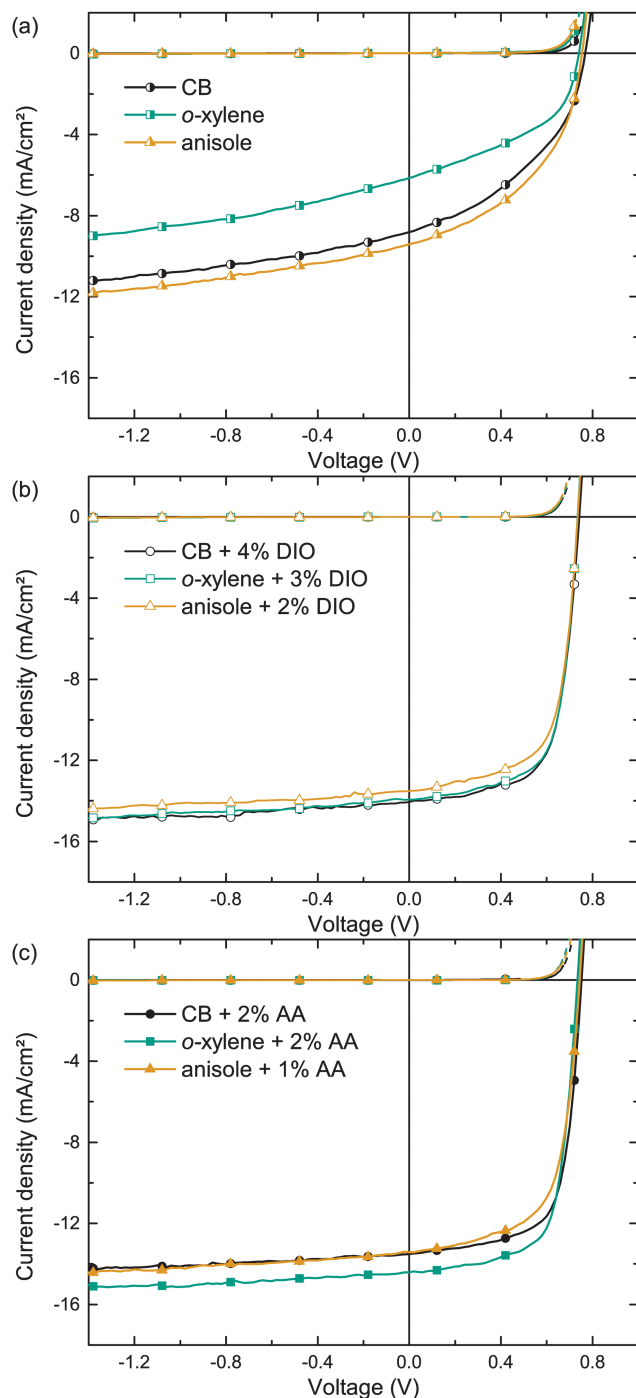
3.1 Device performance

In order to allow comparison with the literature, we initially studied organic solar cells comprising the well investigated polymer:fullerene combination PTB7:PC$_{71}$BM as high performing model systems, enabling PCEs to exceed 7%.[22] Therefore, we utilized the inverted device architecture glass/ITO/ZnO/PTB7:PC$_{71}$BM/MoO$_3$/Ag depicted in Fig. 1. The photo-active layer was spin cast from either o-xylene (boiling point bp = 144 °C), anisole (bp = 154 °C) or, for reference, chlorobenzene (CB, bp = 132 °C). Fig. 2a shows the corresponding current density–voltage (J–V) curves. The key performance data short-circuit current density (J_{sc}), fill factor (FF), open circuit voltage (V_{oc}) and PCE are summarized in Table 2. The moderate photovoltaic device performances (PCE $\approx$ 3%), when using pure solvents, are in accordance with the common literature and reflect the solar cells' moderate J_{sc} and FF.[15,22–24]

Whereas BHJs from pure solvents did not yield efficient polymer solar cells, the addition of the processing additive DIO enhanced both J_{sc} and FF significantly. Fig. 2b depicts the J–V curves of solar cells deposited from CB, o-xylene and anisole with individually optimized DIO concentrations as noted in the graph. The corresponding key performance data are summarized in Table 2. The BHJ deposition from all three solvent/DIO combinations yields high PCEs of $\approx$7% due to an excellent FF >65% and a $J_{sc} \approx$ 14 mA cm^{-2}. Whereas the solar cells that were deposited from pure solvents show different properties, the performance of all devices that were deposited utilizing the additive DIO yields very similar J–V curves. The voltage dependent current densities under reverse bias when using pure solvents indicate poor charge carrier extraction and field dependent recombination. In contrast, upon using the additive DIO, the current density under reverse bias saturates, indicating excellent extraction of free charges and low recombination losses even at low internal fields, being in good agreement with previous studies.[24]

This drastic device performance improvement upon using the additive DIO emphasizes the importance of the solvent additive for efficient PTB7:PC$_{71}$BM solar cells. Although DIO is used in small amounts only, it is a hazardous substance that is not suitable for industrial large-area device processing. Furthermore, DIO residues are suspected to be remaining in the active layer after film formation, due to the high DIO boiling point (bp = 332.5 °C).

Being able to dissolve fullerenes in high concentrations[25] and having a higher boiling point (>200 °C) than most main

2746 | Energy Environ. Sci., 2015, **8**, 2744–2752

This journal is © The Royal Society of Chemistry 2015

Fig. 2 Typical J–V curves of the solar cells under AM1.5 illumination (solid lines) and in the dark (dashed lines) with PTB7:PC$_{71}$BM photo-active layers spin cast from (a) pure solvents, (b) solvent/DIO mixtures and (c) solvent/AA mixtures. The amount of the additive has been optimized for each solvent/additive combination individually (data not provided here). 1 out of 15 data points is marked with a symbol to guide the eye.

solvents, non-halogenated (substituted) benzaldehydes appear as an interesting alternative material class.[26] Being a representative of this material class, we have focused on the eco-compatible additive AA (bp = 248 °C) to improve the formation of the photo-active layer. The J–V curves of the corresponding solar cells

comprising photo-active layers deposited from CB, o-xylene or anisole with an individually optimized additive concentration are shown in Fig. 2c. The key performance data are summarized in Table 2. The drastic PCE enhancement over devices that were deposited from pure main solvents is comparable to the effect of DIO on the device performance. Best J_{sc} and FF were yielded upon BHJ deposition from o-xylene/AA, resulting in an average PCE of 7.4%.

We note that, with respect to future process upscaling, we have performed preliminary doctor blading experiments on PTB7:PC$_{71}$BM in o-xylene/AA solution with the devices yielding similar performance (data not provided here).

3.2 Film characterization

In order to investigate the impact of the solvent/additive combinations on the film formation, we first analyzed the absorption of PTB7:PC$_{71}$BM photo-active layers. Fig. 3 shows the absorbance spectra, which were normalized to the PC$_{71}$BM absorption peak at 377 nm, thereby improving the comparability of the spectra by eliminating minor thickness variations and haze effects. When cast from the pure main solvents CB, o-xylene, or anisole (Fig. 3a), a distinct difference in the polymer absorption profile can be observed: the two local absorption maxima at 680 nm (1) and 630 nm (2) show different relative amplitudes α_1 and α_2. The respective ratios of the 680 nm and 630 nm absorption maxima α_1/α_2 are listed in Table 2. Upon film deposition from CB or anisole, the 680 nm peak is more pronounced than the 630 nm peak, that is, the peak ratio α_1/α_2 is >1, whereas the absorbance of the o-xylene sample at 680 nm is lower than the absorbance at 630 nm and the long wavelength absorption shoulder is less pronounced. The long wavelength absorption shoulder of the polymer usually corresponds to π–π interaction, and a more pronounced absorption shoulder is attributed to an enhanced polymer order.[27,28] We conclude that films cast from o-xylene may exhibit a lower degree of polymer order that hampers charge carrier transport and may therefore partly account for the lower FF and J_{sc} observed on these devices. Upon using either process additive, AA or, for reference, DIO (Fig. 3b), the absorbance spectra were equal within the measurement accuracy and the long wavelength shoulders of all solvent/additive combinations were equally pronounced. The increase in polymer order may foster an improved charge carrier transport and therefore yield a higher FF and J_{sc} which is reflected in the increased α_1/α_2 and which is most pronounced when deposited from o-xylene in combination with either additive.

To further analyze and compare the impact of the solvent additives DIO and AA on the film properties, we studied the film surface topography by atomic force microscopy (AFM) as depicted in Fig. 4. When depositing the PTB7:PC$_{71}$BM film from the pure solvents CB, o-xylene or anisole, we observed protruding nano-spheres with a lateral size of about 150–200 nm and a height of approximately 10–20 nm above the average film surface. For the films cast from o-xylene, these features are even larger, measuring about 300 nm in diameter, with a typical height of about 30 nm. In contrast, when using the additives DIO or AA together with any of the three main

This journal is © The Royal Society of Chemistry 2015

Energy Environ. Sci., 2015, **8**, 2744–2752 | **2747**

Table 2 Key performance data of solar cells comprising PTB7:PC$_{71}$BM photo-active layers cast from different solvent/additive combinations, layer thicknesses t and roughnesses R_q as well as the ratio of the PTB7 absorption maxima (1) and (2), α_1/α_2, as defined in Fig. 2

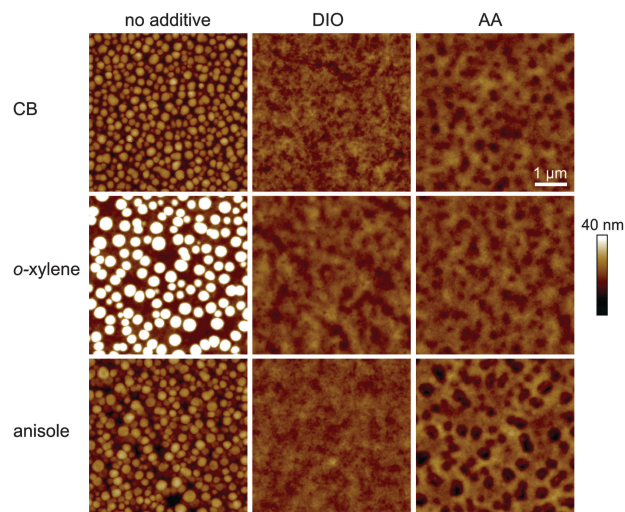| Main solvent	Additive	t (nm)	J_{SC} (mA cm^{-2})	V_{OC} (mV)	FF (%)	PCE^a (%)	R_q (nm)	α_1/α_2
CB	—	90	8.8 ± 0.1	762 ± 7	42 ± 1	2.8 ± 0.1 (2.9)	5.1	1.03
o-Xylene	—	90	6.2 ± 0.2	736 ± 5	45 ± 1	2.0 ± 0.6 (2.2)	12.7	0.96
Anisole	—	80	9.3 ± 0.2	750 ± 1	46 ± 2	3.2 ± 0.2 (3.5)	5.1	1.01
CB	4% DIO	85	14.0 ± 0.1	739 ± 4	67 ± 2	6.9 ± 0.2 (7.3)	2.5	1.07
o-Xylene	3% DIO	85	14.2 ± 0.2	737 ± 5	67 ± 2	7.0 ± 0.2 (7.1)	2.6	1.07
Anisole	2% DIO	80	13.4 ± 0.2	738 ± 3	66 ± 1	6.5 ± 0.1 (6.7)	1.9	1.08
CB	2% AA	90	13.6 ± 0.6	748 ± 5	69 ± 2	7.0 ± 0.3 (7.5)	2.7	1.07
o-Xylene	2% AA	85	14.3 ± 0.1	738 ± 4	70 ± 1	7.4 ± 0.1 (7.6)	2.4	1.07
Anisole	1% AA	80	13.5 ± 0.2	747 ± 4	65 ± 1	6.6 ± 0.2 (6.9)	4.1	1.05

^{a} PCE of the best performing devices in parentheses.
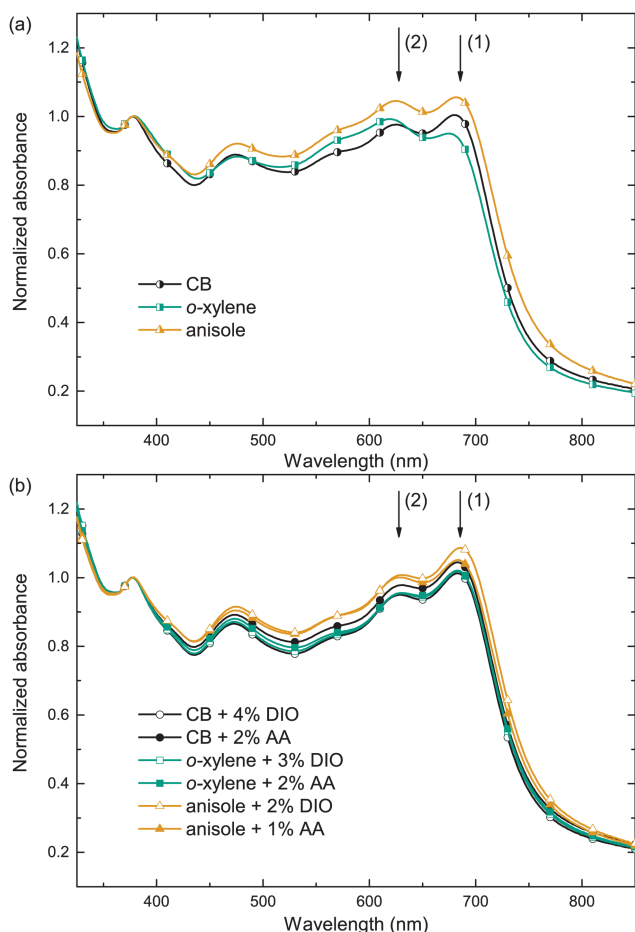
Fig. 3 Absorbance spectra of the PTB7:PC$_{71}$BM layer cast from (a) pure solvents and (b) solvent/additive mixtures. The spectra are normalized to the absorption peak of PC$_{71}$BM at 377 nm. The arrows (1) and (2) indicate the main PTB7 absorption maxima. 1 out of 40 data points is marked with a symbol to guide the eye.

Fig. 4 Topography (AFM, 5 × 5 µm^2) of the PTB7:PC$_{71}$BM photo-active layers cast from different solvent/additive combinations with individually optimized additive concentrations. The same color scale is used for all images. Whereas spherical (fullerene) agglomerates with a diameter of 100–300 nm are clearly visible in films cast from pure solvents, the surface is rather smooth upon addition of DIO or AA to the solution.

solvents, these features are not visible in the AFM images and the surface is rather smooth.

These observations are in good agreement with earlier AFM and transmission electron microscopy (TEM) studies on PTB7:PC$_{71}$BM films that were cast from CB or CB/DIO.[15,22,23] By X-ray diffraction experiments, these spherical features in PTB7:PC$_{71}$BM films were identified to be almost pure fullerene

agglomerates embedded in a polymer:fullerene matrix, with the 200 nm agglomerates when cast from CB being reduced to 30 nm upon deposition from CB/DIO.[23] In additive free bulk-heterojunctions, the fullerene agglomeration therefore leads to enhanced recombination, with the detailed processes still being discussed.[23,24,29] These interpretations match our optoelectronic device study in Section 3.1, where we found reduced recombination as well as enhanced FF and J_{sc} for devices with photo-active layers that were deposited from solvent/DIO or solvent/AA.

We note that we found shallow depression features with a diameter of about 150–300 nm instead (depth 5–10 nm), upon film deposition from CB/AA, o-xylene/AA and, most pronounced, from anisole/AA. Taking into account the excellent performance of the corresponding solar cells, we attribute these features to surface inhomogeneities that form during the drying process rather than material separation.
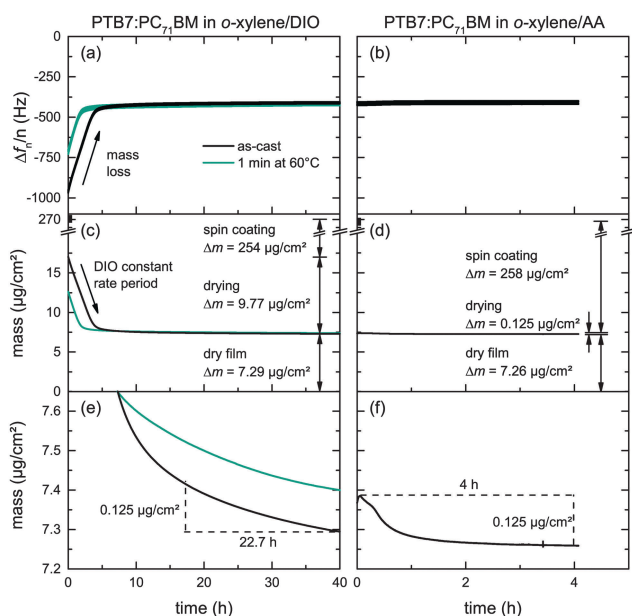
3.3 Drying analysis

The low DIO vapor pressure at room temperature ($p_{DIO}^* = 3.1 \times 10^{-4}$ mbar at $T = 25$ °C)[30] renders DIO practically useless for

2748 | Energy Environ. Sci., 2015, **8**, 2744–2752

This journal is © The Royal Society of Chemistry 2015

large-scale high-throughput fabrication of organic solar cells. Having about the same diffusion coefficient in air ($D_{DIO} = 5.4 \times 10^{-6}$ m^2 s^{-1}, $D_{AA} = 7.1 \times 10^{-6}$ m^2 s^{-1} at $T = 25$ °C)[31] but a higher vapor pressure ($p_{AA}^* = 4.3 \times 10^{-2}$ mbar at $T = 25$ °C) AA appears to be more suitable for fast and complete film drying.

To analyze and compare the drying of PTB7:PC$_{71}$BM/o-xylene solutions containing either additive, DIO or AA (2% v/v), we investigate the evaporation kinetics of additive residues from freshly prepared PTB7:PC$_{71}$BM layers on a quartz crystal microbalance (QCM). On the QCM, we record the resonance frequencies over time. An increasing resonance frequency reflects a loss of mass due to solvent/additive evaporation. Fig. 5a and b shows the relative resonance frequency change of the first harmonics ($n = 1, 3, 5, 7, 9$) $\Delta f_n/n$ of both material systems over time. These resonance frequencies during additive evaporation are given relative to the resonance frequency of the uncoated crystal. We note that the time frame differs by a factor of 10, that is, 40 h for o-xylene/DIO and 4 h for o-xylene/AA. For the as-cast o-xylene/DIO film we find a linearly increasing Δf within the first 5 h of the experiment. During the early stages of drying, henceforth referred to as constant rate period, the thermodynamics at the vapor–liquid interface and the gas-phase mass transport are dominant. The observed linear increase is characteristic of single solvents that evaporate during the constant rate period, inferring that the high-boiling additive DIO is still present in the as-cast film whereas o-xylene has evaporated earlier, during spin casting.

Simultaneous evaporation of two solvents would yield a drying curve that is either non-linear or features a kink at the transition from low- to high-boiling solvent dominated drying.[32,33] At low additive content, that is, at a later stage of drying, which we henceforth refer to as the falling rate period, the diffusion coefficient in polymer solutions can decrease by orders of magnitudes, hampering the removal of trace solvent. The measurements were discontinued after 40 h when only little frequency variation was noted, that is, the film was effectively dry. The experiment was repeated with another film that was annealed on a hotplate (1 min at 60 °C) directly after spin coating, leading to a reduced constant rate period of ≈2 h. Here, after initial sample drying on the hotplate, the subsequent drying at 25 °C shows the same constant evaporation rate as the as-cast film, confirming the presence of only DIO in the film.

In contrast, QCM measurements of films deposited from o-xylene/AA showed almost no frequency change over time and no constant rate period. We conclude that AA had almost completely evaporated earlier, during spin coating.

To quantitatively determine and compare the evaporation rates and the corresponding mass loss from the resonance frequency change, we use the Sauerbrey equation. These mass losses and the corresponding thickness decrease due to additive evaporation are depicted in Fig. 5c and d and summarized in Table 3 for both solvent mixtures versus time. Fig. 5e and f shows a zoom in the relevant mass regime of the falling rate period. Within 4 hours of drying, about 125 ng cm^{-2} of the additive AA evaporated from the PTB7:PC$_{71}$BM film at room temperature, yielding an average evaporation rate of 31 ng cm^{-2} h^{-1}. In contrast, it takes 22.7 hours for the same amount of DIO to evaporate, yielding an average evaporation rate of 5.5 ng cm^{-2} h^{-1}. Only at the end of the measurements, that is, after 4 h of AA evaporation and 40 h of DIO evaporation, the evaporation rates of both additives have equalized (2.5 ng cm^{-2} h^{-1}). If we assume additive diffusion within the film to limit the additive evaporation and a dry film at the end of the experiment, we can conclude that the diffusion coefficient of DIO is lower than the diffusion coefficient of AA in the PTB7:PC$_{71}$BM matrix.

Moreover, the relationship of mass with frequency change allows for calculating the film thickness of the dry layers t_{dry}. In all experiments the frequencies $\Delta f_n/n$ approached about −410 Hz

Fig. 5 Drying characteristics of PTB7:PC$_{71}$BM at 25 °C cast from o-xylene/DIO and o-xylene/AA (2% v/v). (a and b) QCM measurements after spin coating. The changes in the resonance frequencies reflect mass loss. (c and d) Drying curves calculated from the QCM frequency change using the Sauerbrey equation. Whereas only very little mass loss is observed for o-xylene/AA films, o-xylene/DIO films show a constant initial mass decrease, characteristic of evaporation of the additive at the vapor–liquid interface. (e and f) Zoom into the relevant mass regime of the falling rate period of the drying curve, where the mass loss is determined by the diffusion of the additive inside the PTB7:PC$_{71}$BM matrix. AA diffuses faster than DIO.

Table 3 Residual solvent mass and the corresponding layer thickness differences ($t-t_{dry}$) of PTB7:PC$_{71}$BM thin-films cast from o-xylene/DIO or o-xylene/AA (2% v/v) versus drying time

Additive	Drying time (h)	Solvent mass $\Delta m-\Delta m_{dry}$ (ng cm^{-2})	Thickness difference $t-t_{dry}$ (nm)
DIO	0	9766	53
	5	600	3.5
	10	244	1.5
	20	101	0.8
	30	41	0.4
	40	0	0
AA	0	125	1.1
	2	6	0.2
	4	0	0

This journal is © The Royal Society of Chemistry 2015

Energy Environ. Sci., 2015, **8**, 2744–2752 | **2749**

at the end of the measurement procedures, which corresponds to a dry film thickness of 60 nm, assuming a density of 1.2 g cm^{-3} for typical organic semiconductors.[34] This allowed us to determine the mass of the initial wet layer before solvent and additive evaporation, taking into account the initial composition of the PTB7:PC$_{71}$BM/o-xylene/additive solutions and the respective densities. After spin coating, about 96 wt% of the o-xylene/DIO solution had evaporated from the PTB7:PC$_{71}$BM layer, whereas 99.9 wt% of the o-xylene/AA solution had evaporated under equal conditions.

3.4 Other photo-active polymers

To demonstrate the general applicability of the o-xylene/AA solvent combination for the fabrication of highly efficient organic solar cells, we transferred the deposition process to various other commercially available polymer:fullerene blends that are known to perform very well after deposition from common hazardous halogenated solvents. We note that the commercially available polymers may have a different molecular weight than the respective polymers in earlier reports and may therefore yield a somewhat different device performance.

As a structural advancement of PTB7, the polymer PTB7-Th was reported in the literature, enabling enhanced PCEs exceeding 9%, when deposited from CB/DIO on top of a modified ZnO interfacial layer, or yielding PCEs of more than 10%, when using an organic interlayer instead.[35,36] Following the experimental protocol of Section 3.1, the J–V curves of these solar cells deposited from either CB/DIO, o-xylene or o-xylene/AA are depicted in Fig. 6. All key performance data are listed in Table 4. Whereas PTB7-Th:PC$_{71}$BM reference solar cells cast from CB and 4% DIO (v/v) show PCEs of 7.5%, which is in good agreement with literature known results on plain ZnO,[35] the PCEs of solar cells that were processed from o-xylene and 2% AA (v/v) improved to 8.3%.

Similar observations were made for photo-active blends comprising the narrow bandgap polymer PDTP-DFBT and PC$_{71}$BM, which can yield PCEs of up to 8% when cast from pure o-DCB,[37] and which were also employed in highly efficient tandem solar cells.[38–40] It was pointed out in the literature that the deposition of PDTP-DFBT:PC$_{71}$BM BHJs from o-DCB, omitting any additives, is sufficient to yield high PCEs. However, we found that this concept does not apply to the deposition from the non-chlorinated solvent o-xylene. In contrast, adding AA to the o-xylene solution (1.5% v/v), we yielded PDTP-DFBT:PC$_{71}$BM (1:1.5) solar cells with PCEs of up to 5.0%, clearly outperforming both reference devices deposited from pure o-DCB (PCE = 4%, blend ratio 1:2) or o-xylene (PCE = 1%). We note that we found significantly higher PDTP-DFBT solubility in o-xylene than in o-DCB, making o-xylene – besides the environmental aspect – much more favorable towards improved processability of this polymer.
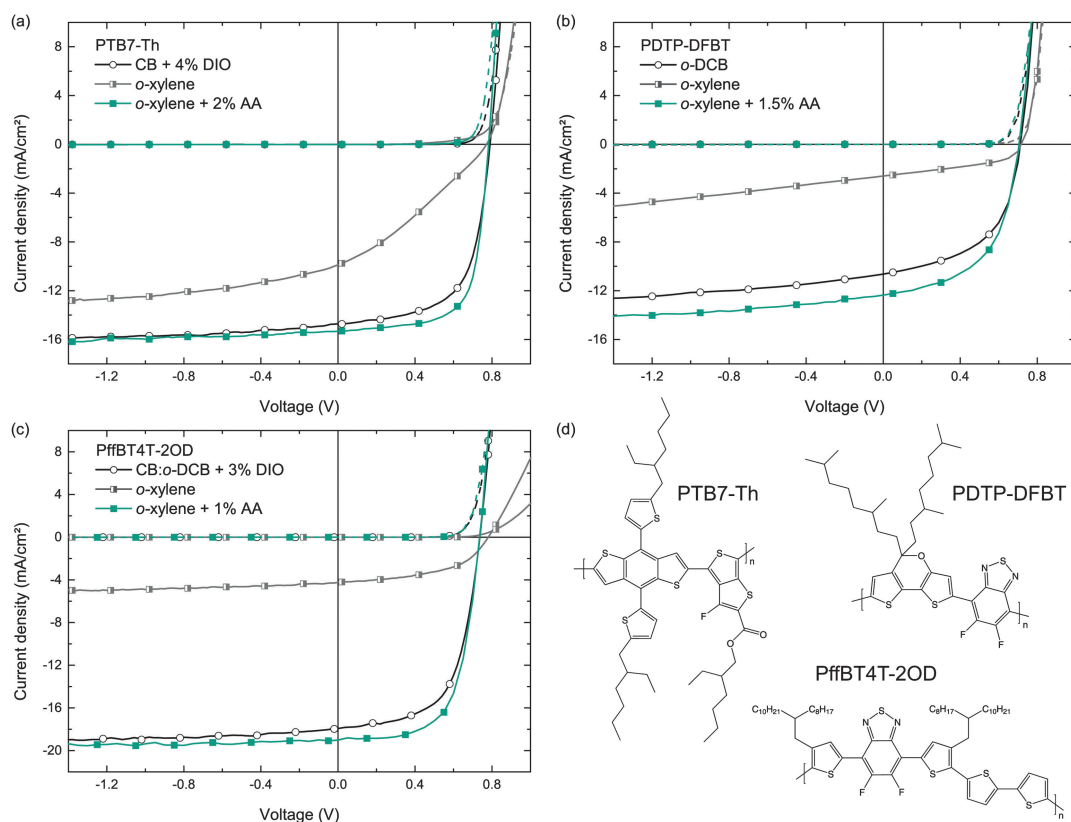

Fig. 6 Typical J–V curves of solar cells with high-performance polymer:PC$_{71}$BM BHJs comprising the polymers (a) PTB7-Th, (b) PDTP-DFBT and (c) PffBT4T-2OD, all deposited from o-xylene/AA. Dashed lines represent the J–V curves in the dark. 1 out of 10 data points is marked with a symbol to guide the eye. (d) Chemical structures of the photo-active polymers.

Table 4 Key performance data of solar cells comprising various polymer:PC$_{71}$BM blends cast from different solvent/additive combinations. Furthermore, the blending ratio with PC$_{71}$BM, the polymer concentration in solution c and the photo-active layer thickness t are listed

Polymer	Blend ratio	c (g L^{-1})	Main solvent	Additive	t (nm)	J_{SC} (mA cm^{-2})	V_{OC} (mV)	FF (%)	PCE^a (%)
PTB7-Th	1:1.5	10	CB	4% DIO	125	15.1 ± 0.2	791 ± 3	62 ± 1	7.5 ± 0.1 (7.6)
	1:1.5	10	o-Xylene	—	120	10.0 ± 0.1	772 ± 1	31 ± 1	2.3 ± 0.1 (2.4)
	1:1.5	10	o-Xylene	2% AA	100	15.3 ± 0.2	783 ± 1	69 ± 1	8.3 ± 0.1 (8.5)
PDTP-DFBT	1:2	8	o-DCB	—	95	10.6 ± 0.2	712 ± 3	53 ± 1	4.0 ± 0.1 (4.2)
	1:1.5	9.6	o-Xylene	—	90	2.6 ± 0.1	720 ± 4	45 ± 1	0.9 ± 0.1 (0.9)
	1:1.5	9.6	o-Xylene	1.5% AA	105	12.4 ± 0.1	704 ± 5	54 ± 1	4.7 ± 0.2 (5.0)
PffBT4T-2OD	1:1.2	10	CB:o-DCB 1:1	3% DIO	440	17.5 ± 0.4	736 ± 3	60 ± 1	7.7 ± 0.3 (8.1)
	1:1.2	9	o-Xylene	—	450	4.0 ± 0.2	775 ± 15	48 ± 2	1.5 ± 0.1 (1.7)
	1:1.2	9.5	o-Xylene	1% AA	300^b	18.0 ± 1.0	738 ± 3	68 ± 3	9.0 ± 0.2 (9.5)

^{a} PCE of the best performing device in parentheses. ^{b} Cells with up to 600 nm thickness and similar device performance.

As a third example, we investigated o-xylene/AA for the deposition of a blend comprising PffBT4T-2OD and PC$_{71}$BM. Very recently, this polymer was reported to enable PCEs exceeding 10%. It exhibits high crystallinity and performs very well in thick active layers ($\approx$300 nm).[1] Following the previously published preparation protocol, we built reference solar cells incorporating a PffBT4T-2OD:PC$_{71}$BM photo-active blend from a CB:o-DCB 1:1 solvent mixture with the addition of 3% DIO, resulting in an average device efficiency of 7.7%. Using the solvent o-xylene plus 1% of AA instead, we yielded PCEs of 9.0% (hero device: 9.5%), with the improvement originating mainly from a higher FF. Again, without employing AA, the efficiency of the solar cells is drastically lower.

4. Conclusions

The eco-compatible solvent/additive combination o-xylene/AA is an excellent alternative to the commonly used halogenated and environmentally harmful CB/DIO for the deposition of a broad selection of highly efficient polymer:PC$_{71}$BM bulk-heterojunctions. The corresponding solar cells outperform the reference devices, yielding up to 9.5% power conversion efficiency (PffBT4T-2OD:PC$_{71}$BM). As compared to DIO, the higher volatility of the additive AA reduces the drying time of the photo-active layer significantly, enabling smaller drying ovens or higher web-speeds for future roll-to-roll fabrication plants.

Acknowledgements

Notes and references

1 Y. Liu, J. Zhao, Z. Li, C. Mu, W. Ma, H. Hu, K. Jiang, H. Lin, H. Ade and H. Yan, *Nat. Commun.*, 2014, **5**, 5293.
2 F. C. Krebs and M. Jørgensen, *Sol. Energy Mater. Sol. Cells*, 2013, **119**, 73.
3 R. Po, A. Bernardi, A. Calabrese, C. Carbonera, G. Corso and A. Pellegrino, *Energy Environ. Sci.*, 2014, **7**, 925.
4 O. Synooka, K.-R. Eberhardt and H. Hoppe, *RSC Adv.*, 2014, **4**, 16681.
5 B. R. Aïch, S. Beaupré, M. Leclerc and Y. Tao, *Org. Electron.*, 2014, **15**, 543.
6 P.-T. Tsai, C.-Y. Tsai, C.-M. Wang, Y.-F. Chang, H.-F. Meng, Z.-K. Chen, H.-W. Lin, H.-W. Zan, S.-F. Horng, Y.-C. Lai and P. Yu, *Org. Electron.*, 2014, **15**, 893.
7 C.-C. Chueh, K. Yao, H.-L. Yip, C.-Y. Chang, Y.-X. Xu, K.-S. Chen, C.-Z. Li, P. Liu, F. Huang, Y. Chen, W.-C. Chen and A. K.-Y. Jen, *Energy Environ. Sci.*, 2013, **6**, 3241.
8 K.-S. Chen, H.-L. Yip, C. W. Schlenker, D. S. Ginger and A. K.-Y. Jen, *Org. Electron.*, 2012, **13**, 2870.
9 S. Venkatesan, Q. Chen, E. C. Ngo, N. Adhikari, K. Nelson, A. Dubey, J. Sun, V. Bommisetty, C. Zhang, D. Galipeau and Q. Qiao, *Energy Technol.*, 2014, **2**, 269.
10 A. Lange, W. Schindler, M. Wegener, K. Fostiropoulos and S. Janietz, *Sol. Energy Mater. Sol. Cells*, 2013, **109**, 104.
11 G. Susanna, L. Salamandra, C. Ciceroni, F. Mura, T. M. Brown, A. Reale, M. Rossi, A. Di Carlo and F. Brunetti, *Sol. Energy Mater. Sol. Cells*, 2015, **134**, 194.
12 J. K. Lee, W. L. Ma, C. J. Brabec, J. Yuen, J. S. Moon, J. Y. Kim, K. Lee, G. C. Bazan and A. J. Heeger, *J. Am. Chem. Soc.*, 2008, **130**, 3619.
13 N. Shin, L. J. Richter, A. a. Herzing, R. J. Kline and D. M. DeLongchamp, *Adv. Energy Mater.*, 2013, **3**, 938.
14 L. J. Richter, D. M. DeLongchamp, F. a. Bokel, S. Engmann, K. W. Chou, A. Amassian, E. Schaible and A. Hexemer, *Adv. Energy Mater.*, 2015, **5**, 1400975.
15 F. Liu, W. Zhao, J. R. Tumbleston, C. Wang, Y. Gu, D. Wang, A. L. Briseno, H. Ade and T. P. Russell, *Adv. Energy Mater.*, 2014, **4**, 1301377.
16 J. J. van Franeker, M. Turbiez, W. Li, M. M. Wienk and R. A. J. Janssen, *Nat. Commun.*, 2015, **6**, 6229.

17 J. Peet, J. Y. Kim, N. E. Coates, W. L. Ma, D. Moses, A. J. Heeger and G. C. Bazan, *Nat. Mater.*, 2007, **6**, 497.

18 Y. Kim, H. R. Yeom, J. Y. Kim and C. Yang, *Energy Environ. Sci.*, 2013, **6**, 1909.

19 X. Guo, M. Zhang, C. Cui, J. Hou and Y. Li, *ACS Appl. Mater. Interfaces*, 2014, **6**, 8190.

20 W. Zhao, L. Ye, S. Zhang, M. Sun and J. Hou, *J. Mater. Chem. A*, 2015, **3**, 12723.

21 I. Reviakine, D. Johannsmann and R. P. Richter, *Anal. Chem.*, 2011, **83**, 8838.

22 Y. Liang, Z. Xu, J. Xia, S.-T. Tsai, Y. Wu, G. Li, C. Ray and L. Yu, *Adv. Mater.*, 2010, **22**, E135.

23 B. A. Collins, Z. Li, J. R. Tumbleston, E. Gann, C. R. McNeill and H. Ade, *Adv. Energy Mater.*, 2013, **3**, 65.

24 A. Foertig, J. Kniepert, M. Gluecker, T. Brenner, V. Dyakonov, D. Neher and C. Deibel, *Adv. Funct. Mater.*, 2014, **24**, 1306.

25 I. Burgués-Ceballos, F. Machui, J. Min, T. Ameri, M. M. Voigt, Y. N. Luponosov, S. A. Ponomarenko, P. D. Lacharmoise, M. Campoy-Quiles and C. J. Brabec, *Adv. Funct. Mater.*, 2014, **24**, 1449.

26 R. Tuttle, M. L. Reitz and B. E. Woodworth, *US Pat.*, 20100043876A1, 2010.

27 H.-Y. Chen, J. Hou, A. E. Hayden, H. Yang, K. N. Houk and Y. Yang, *Adv. Mater.*, 2010, **22**, 371.

28 J. A. Bartelt, J. D. Douglas, W. R. Mateker, A. El Labban, C. J. Tassone, M. F. Toney, J. M. J. Fréchet, P. M. Beaujuge and M. D. McGehee, *Adv. Energy Mater.*, 2014, **4**, 1301733.

29 G. J. Hedley, A. J. Ward, A. Alekseev, C. T. Howells, E. R. Martins, L. A. Serrano, G. Cooke, A. Ruseckas and I. D. W. Samuel, *Nat. Commun.*, 2013, **4**, 2867.

30 C. L. Yaws, *The Yaws Handbook of Vapor Pressure: Antoine Coefficients*, 1st edn, 2007.

31 *VDI Heat Atlas, VDI-Gesellschaft Verfahrenstechnik und Chemieingenieurwesen*, Springer-Verlag, Berlin, Heidelberg, 2010.

32 B. Schmidt-Hansberg, M. Baunach, J. Krenn, S. Walheim, U. Lemmer, P. Scharfer and W. Schabel, *Chem. Eng. Process.*, 2011, **50**, 509.

33 B. Schmidt-Hansberg, M. Sanyal, N. Grossiord, Y. Galagan, M. Baunach, M. F. G. Klein, A. Colsmann, P. Scharfer, U. Lemmer, H. Dosch, J. Michels, E. Barrena and W. Schabel, *Sol. Energy Mater. Sol. Cells*, 2012, **96**, 195.

34 J. W. Kiel, B. J. Kirby, C. F. Majkrzak, B. B. Maranville and M. E. Mackay, *Soft Matter*, 2010, **6**, 641.

35 S.-H. Liao, H.-J. Jhuo, Y.-S. Cheng and S.-A. Chen, *Adv. Mater.*, 2013, **25**, 4766.

36 Z. He, B. Xiao, F. Liu, H. Wu, Y. Yang, S. Xiao, C. Wang, T. P. Russell and Y. Cao, *Nat. Photonics*, 2015, **9**, 174.

37 L. Dou, C. Chen, K. Yoshimura, K. Ohya, W. Chang, J. Gao, Y. Liu, E. Richard and Y. Yang, *Macromolecules*, 2013, **46**, 3384.

38 J. You, L. Dou, K. Yoshimura, T. Kato, K. Ohya, T. Moriarty, K. Emery, C.-C. Chen, J. Gao, G. Li and Y. Yang, *Nat. Commun.*, 2013, **4**, 1446.

39 J. You, C.-C. Chen, Z. Hong, K. Yoshimura, K. Ohya, R. Xu, S. Ye, J. Gao, G. Li and Y. Yang, *Adv. Mater.*, 2013, **25**, 3973.

40 C.-C. Chen, W.-H. Chang, K. Yoshimura, K. Ohya, J. You, J. Gao, Z. Hong and Y. Yang, *Adv. Mater.*, 2014, **26**, 5670.

2752 | *Energy Environ. Sci.*, 2015, **8**, 2744–2752

This journal is © The Royal Society of Chemistry 2015